Particle & Particle Systems Characterization
www.particle-journal.com

Green Chemical Approach for the Synthesis of ZnO Nanoparticles and Investigation of their Cytotoxicity

*Hemra Hamrayev, Seyed Davoud Jazayeri, Mostafa Yusefi, Brianna, Sin-Yeang Teow, Yuan Seng Wu, Ayaz Anwar, Serdar Korpayev, Aras Kartouzian, and Kamyar Shameli**

In this study, zinc oxide nanoparticles (ZnO-NPs) are synthesized and combined with chitosan (Cs) to create Cs/ZnO-NPs nanomicelles, aiming to investigate their potential as a novel cancer treatment. The ZnO-NPs are produced through a sintering process at temperatures ranging from 300 to 700 °C. The most effective nanoparticles are obtained at 600 °C, as determined by X-ray diffraction (XRD) and Fourier-transform infrared spectroscopy (FTIR) analyses, which confirmed their crystallinity and purity. Transmission electron microscopy (TEM) and scanning electron microscopy (SEM) are employed to characterize the size and shape of the nanoparticles, revealing predominantly spherical and hexagonal structures with stable dimensions. The cytotoxic effects of the Cs/ZnO-NPs are evaluated against various cancer cell types. The results show that at a concentration of 125 µg mL^{-1}, the Cs/ZnO-NPs demonstrate significantly higher cancer cell toxicity compared to ZnO-NPs alone, while remaining non-toxic to normal cells. This indicates that Cs/ZnO-NPs have a superior ability to selectively target cancer cells. These findings suggest that Cs/ZnO-NPs nanomicelles hold promise as an effective and safe nanotherapeutic approach in the realm of cancer treatment, meriting further exploration for clinical applications.

1. Introduction

Nanotechnology has become a significant and appealing area of research, offering distinct features and broad applications in diverse sectors including agriculture, food, and biomedicine. The properties attributed to nanoparticles, such as their small size, large surface area to volume ratio, and versatile optical, magnetic, chemical, and mechanical characteristics, have positioned them as promising candidates for pioneering applications in biomedicine. Their well-documented effectiveness as antibiotic, antioxidant, and anticancer agents underscores their potential in this field.[1] Zinc oxide nanoparticles (ZnO-NPs) are an attractive choice for numerous biomedical applications as inorganic semiconductors. They possess favorable characteristics such as a substantial binding energy, a wide bandgap, a hexagonal wurtzite crystal structure, and notable anticancer

H. Hamrayev
Malaysia-Japan International Institute of Technology
Universiti Teknologi Malaysia
Kuala Lumpur 54100, Malaysia

S. D. Jazayeri
School of Biochemistry and Immunology
Trinity Biomedical Sciences Institute
Trinity College Dublin
Dublin 2, Ireland

M. Yusefi
Institute of Biological Sciences
Faculty of Science
Universiti Malaya
Kuala Lumpur 50603, Malaysia

Brianna
Department of Medical Sciences
School of Medical and Life Sciences
Sunway University
Selangor Darul Ehsan 47500, Malaysia

S.-Y. Teow
Department of Biology
College of Science
Mathematics and Technology
Wenzhou-Kean University
Zhejiang 325060, China

S.-Y. Teow
Wenzhou Municipal Key Laboratory for Applied Biomedical and Biopharmaceutical Informatics
Ouhai, Wenzhou, Zhejiang 325060, China

S.-Y. Teow
Zhejiang Bioinformatics International Science and Technology Cooperation Center
Ouhai, Wenzhou, Zhejiang 325060, China

S.-Y. Teow
Dorothy and George Hennings College of Science
Mathematics and Technology
Kean University
1000 Morris Ave, Union, NJ 07083, USA

The ORCID identification number(s) for the author(s) of this article can be found under https://doi.org/10.1002/ppsc.202400009

DOI: 10.1002/ppsc.202400009

and antibacterial properties.[2,3] The US Food and Drug Administration (in accordance with 21CFR182.8991) and various scientific studies affirm ZnO's safety and biocompatibility, making it a promising material for treating conditions like kidney diseases, ischemic ailments, microbial and fungal infections, cardiovascular disease, diabetes, and cancer.[4–7]

ZnO-NPs can be produced through various methods, including solvothermal and hydrothermal processes,[8] precipitation,[9,10] polymerization,[11] laser ablation,[12] sonochemical techniques,[13] sol–gel synthesis,[14,15] and microwave-assisted approaches.[16] Among these methods, the sol–gel procedure has garnered significant attention due to its ability to tailor the shape, physicochemical properties, and patterning of ZnO nanostructures effectively.[17]

The utilization of green materials has gained popularity in the production of metal and metal oxide nanoparticles (NPs), including ZnO-NPs.[18] For instance, extracts from *Ailanthus altissima* fruit,[19] *phoenix dactylifera* waste,[20] *Lawsonia inermis* plant,[21] *Punica granatum*,[22] and *Justicia procumbense* leaves,[23] have recently been employed in the eco-friendly green synthesis of ZnO-NPs. Furthermore, high molecular weight macromolecules like polysaccharide hydrocolloids (such as alginate, starches, pectin, pullulan, and gums) are readily available and offer a sustainable approach to the green synthesis of ZnO-NPs.[24]

The utilization of a green sol-gel approach, coupled with high calcination temperatures and the involvement of biopolymer mediators, represents a less hazardous and more eco-friendly strategy for synthesizing biocompatible ZnO-NPs. During the green synthesis process, biopolymer components could not only hydrolyze metal salt solution but also present onto the metal NPs to decrease particle agglomeration to improve thermodynamic stability, water permeability, biocompatibility, biodegradability, and tolerable toxicity.[25–27,22]

Carrageenan, a naturally occurring linear polysaccharide derived from marine red seaweeds, is gaining prominence as an environmentally friendly choice in the food industry, where it serves as a crucial gelling and stabilizing agent.[28,29] Specifically, κ-carrageenan, a sulfated polysaccharide, stands out due to its distinctive linear composition, which consists of D-galactose and 3,6-anhydro-D-galactose units.

The intrinsic biological activity of carrageenan as a natural polysaccharide has led to a substantial upswing in its human-oriented uses, attributed to its specific chemical and physical attributes. Harnessing its affordability and the presence of a negatively charged backbone, κ-carrageenan demonstrates its effectiveness in the synthesis of ZnO-NPs by serving as both a stabilizing and capping agent.[30,24]

This biopolymer finds application in altering the surface properties of both metal and metal oxide NPs.[31] Coating by biopolymers such as chitosan (Cs) with a positively charged backbone can increase the dispersion and colloidal stability of NPs to improve antimicrobial and anticancer effects.[32] Chitosan, a naturally occurring amino-polysaccharide, can be derived from chitin. It possesses a linear structure and carries a positive charge, making it a cationic substance.[33] In medically-related applications, chitosan with high biocompatibility and water-rich structure can be used as a coating agent for ZnO-NPs.[34,35] Albeit, it should be noted that the polymer coating procedure could be complicated, laborious, and time-consuming.[36] Of this, the simple and quick immersing of the ZnO-NPs in the chitosan solution could form a thin chitosan layer around the NPs to enhance the biocompatibility and biodegradability of the NPs.[37,38]

Traditional cancer therapies, including chemotherapy and radiotherapy, are associated with adverse effects that can cause harmful side effects. These effects may encompass symptoms like vomiting, delirium, insomnia, fatigue, and nausea.[39] To overcome these problems, the utilization of polymeric metal nano-complexes presents a promising avenue for improving factors such as circulation duration, targeted therapeutic efficacy, and the safe delivery of drugs. Interestingly, -OH groups of the ZnO surface lead to gently dissolving ZnO in both the acidic- and basic environments.[40] Thus, ZnO and ZnO coated by biopolymer have gained immense interest for potent anticancer actions against various cancer cells, including breast MCF-7.[41] gastric AGS,[42] cervical HeLa,[43] liver Hep-G2,[21] and colorectal HCT116,[44] and caco-2.[45]

Considering the anticancer properties of Zn, ZnO-NPs received much attention in recent years. Some studies indicated that ZnO-NPs could target the critical mechanisms of cancer chemoresistance and enhance the effectiveness of chemotherapy drugs. These studies showed that ZnO-NPs reduced the activity of ATP-binding cassette (ABC) transporters, increased DNA damage and apoptosis, and attenuated stemness in cancer cells, leading to enhanced chemo-sensitivity. Other studies also demonstrated that ZnO-NPs in low doses were helpful in minimizing the harmful side effects of chemotherapy drugs.[46] Hu et al. found ZnO-NPs induced autophagy, causing tumor cell death via intracellular dissolution and reactive oxygen species (ROS) generation. They promoted autophagy related 5-regulated autophagy flux, resulting in cancer cell death. Co-localization with autophagic vacuoles indicated ZnO-NPs' link to autophagy. ZnO-NPs enhanced chemotherapy efficacy and overcame drug resistance.[47]

Y. S. Wu
Centre for Virus and Vaccine Research
School of Medical and Life Sciences
Sunway University
Selangor Darul Ehsan 47500, Malaysia
A. Anwar
Department of Biological Sciences
School of Medical and Life Sciences
Sunway University
Selangor Darul Ehsan 47500, Malaysia
S. Korpayev
Biotechnology Institute
Ankara University
Ankara 06100, Turkey
A. Kartouzian
Catalysis Research Center and School of Natural Science
Technical University of Munich
85747 Garching, Germany
K. Shameli
Institute of Virology
School of Medicine
Technical University of Munich
85747 Munich, Germany
E-mail: kamyar.shameli@tum.de

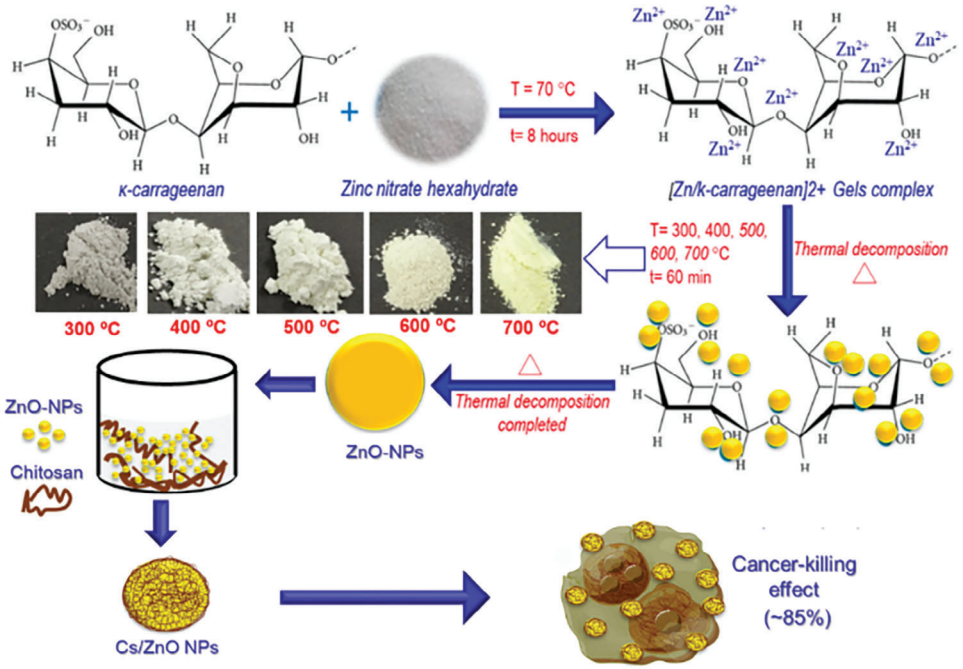

Figure 1. Schematic illustration of ZnO-NPs synthesis and chitosan coating process aimed at increasing cytotoxic effects on cancer cells.

This study aims to fabricate ZnO-NPs and Cs/ZnO-NPs and to investigate their physiochemical and cytotoxic effects against cancer cells. Utilizing carrageenan as the polymeric medium, a green chemical approach was utilized for ZnO-NPs synthesis, offering the flexibility to finely tune NPs size by adjusting the reaction sintering process. Following the production of nanomicelles composed of Cs/ZnO-NPs, a subsequent step involved immersing these fabricated ZnO-NPs in a solution containing Cs. Thorough characterization of the synthesized NPs was conducted using a comprehensive array of techniques, including XRD, UV–vis, SEM, TEM, EDS, FTIR, and TGA, as well as assessments of zeta potential (ζ-potential) and polydispersity indices. The underlying hypothesis posits that both ZnO-NPs (S4) and the corresponding Cs/ZnO-NPs nanomicelles would exhibit noteworthy cytotoxicity against various cancer cell types. Particularly notable is the anticipation that Cs/ZnO-NPs would outperform ZnO-NPs in their ability to trigger cellular demise, emphasizing their potential as a more formidable strategy in the fight against cancer. To further investigate, the in vitro assessment extended to appraising the samples' toxicity on breast, lung and muscular cancer cells, in comparison with embryonic normal kidney cells.

2. Results and Discussion

In this current investigation, we employed the sol-gel method to synthesize ZnO-NPs, as illustrated in **Figure 1**. During this procedure, the vinyl sulfonic acid functional groups within carrageenan engage with the Zn^{2+} ions.[30] When the zinc nitrate solution is mixed with carrageenan solution, the OH groups can interact with the metal cations. The heating declines the presence of water and the smaller amylose molecules cause the formation of a network with water to enhance the mixture's viscosity.[48]

This procedure is named carrageenan gelatinization. Finally, the zinc nitrate decomposed to oxygen and nitrogen dioxide during the heating process and was subsequently eliminated from the mixtures. As depicted in Figure 1, the color of the ZnO-NPs obtained through the sol-gel process underwent a transformation as the calcination temperature increased from 300 to 700 °C. To create a simple and environmentally friendly composite, ZnO-NPs annealed at 600 °C were immersed in a chitosan solution, resulting in Cs/ZnO-NPs.

2.1. X-Ray Diffraction (XRD) Analysis

The XRD results (**Figure 2**) revealed distinct peaks at 2θ values 32.00°, 34.53°, 36.35°, 47.65°, 56.68°, 63.05°, 66.53°, 68.05°, and 69.27° for ZnO-NPs which are attributed to (100), (101), (002), (102), (110), (103), (200), (112), and (201) crystal planes, respectively. These data clearly signify the formation of the ZnO wurtzite structure (JCPDS #036-1451).[22] Different calcination temperatures applied to ZnO-NPs can lead to the intensity growth of the peaks associated with distinct crystalline sizes. For example, Equation (1)-based calculation estimated the crystallite size of 25 ± 35, 29 ± 61, 35 ± 31, 42 ± 26, and 42 ± 73 nm for the samples S1–S5, respectively. Consistent findings have been reported in a separate study.[48] Based on the XRD data; the crystalline size exhibited an upward trend with increasing the calcination temperature up to 600 °C.

2.2. UV–vis Spectroscopy Analysis

Utilizing the UV–vis data depicted in **Figure 3a**, it is evident that ZnO-NPs subjected to calcination at 300 °C (S1) exhibited

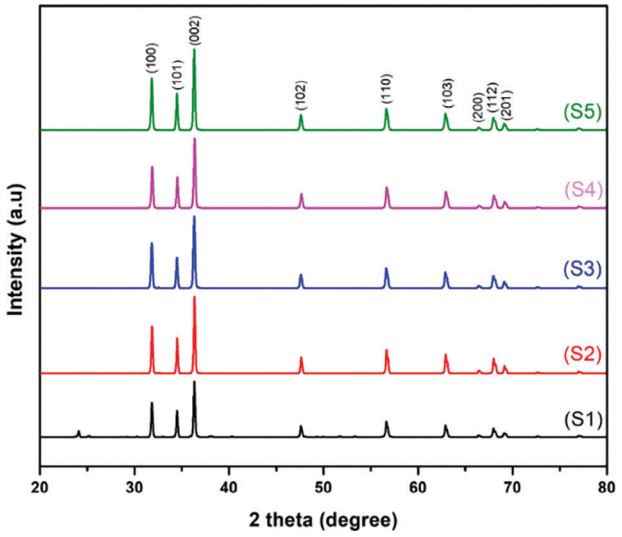

Figure 2. XRD data of ZnO-NPs calcined at 300, 400, 500, 600, and 700 °C (S1–S5), respectively.

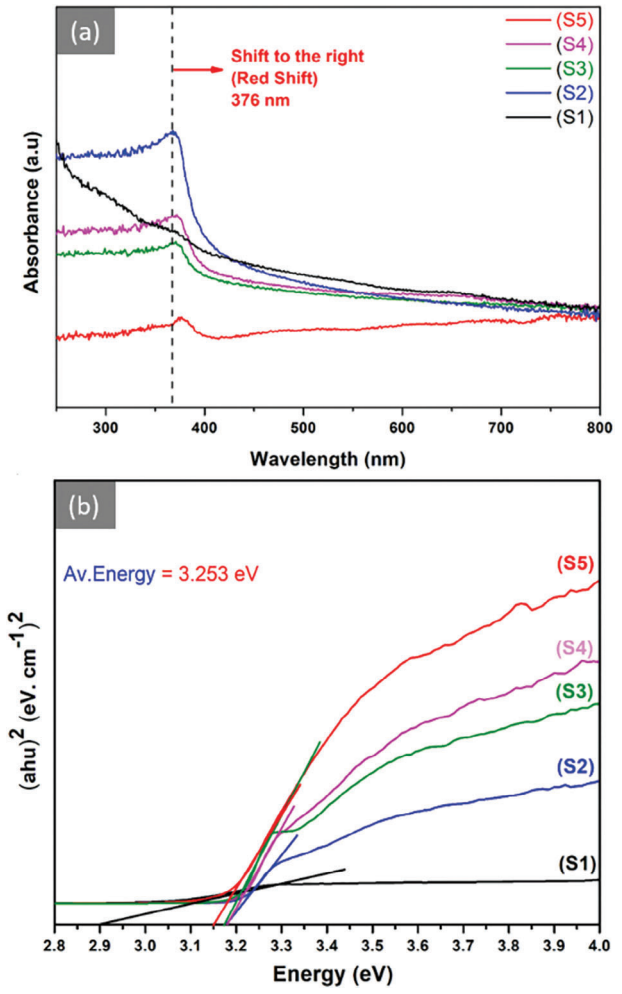

Figure 3. a) UV–vis absorption spectrum and b) bandgap energy of ZnO-NPs calcined at 300, 400, 500, 600, and 700 °C for the S1-S5 samples, respectively.

a notably low UV–vis peak intensity. In contrast, ZnO-NPs that underwent calcination at 400, 500, 600, and 700 °C (S2–S5) displayed distinct absorption peaks at 369, 371, 372, and 376 nm, respectively.

This is related to the characteristic band associated with the synthesized ZnO, occurring at a wavelength of 370 nm. This phenomenon results from electron transitions occurring between the valence band and the conduction band, specifically involving O2p and Zn3d orbitals.[49] This peak indicates that the particles are in the nano-size range, and the distribution of particle size is narrow.[48] The data showed that as calcination temperature increases, the wavelength value for S2–S5 also increases.[50] Figure 3b indicates the presence of a bandgap in the absorbance spectra of the ZnO-NPs. The magnitude of this gap can be ascertained from the absorbance spectra by computing the derivative of absorbance concerning photon energy and pinpointing the peak in the derivative spectrum situated at the lower-energy region. The S1-S5 samples indicated the bandgap values of 3.221, 3.251, 3.258, 3.268, and 3.265 eV, respectively, which are comparable to the bandgap energy values of bulk ZnO (3.29 eV).[51]

2.3. Thermal Analysis

The findings from the TGA and differential thermogravimetric analysis (DTGA) are presented in **Figure 4**, indicating the final residue of 85.58, 98.34, 99.02, 98.13, and 99.74 weight% at 800 °C for the S1–S5 samples, respectively. The first and the second weight loss could be due to the presence of water and the decomposition of chemically bound groups, respectively.

The third and final step is attributed to the decomposition of the organic groups and the formation of the pyrochlore phases.48 These data indicated that the thermal stability of the samples was attributed to the presence of ZnO-NPs.

2.4. Fourier Transform Infrared Spectroscopy (FTIR) Analysis

FTIR spectroscopy determines the presence of functional groups in the synthesized samples. Carrageenan exhibits strong peaks in the 1200–1250 cm^{-1} and 800–900 cm^{-1} regions, representing the stretching vibrations of the sulfate (SO_4) groups present in its structure. Carrageenan exhibited peaks ≈1040–1080 cm^{-1}, indicating the presence of glycosidic linkages (C—O—C) in the structure. Furthermore, characteristic peaks within the range of 900–1000 cm^{-1} may correspond to the anhydrogalactose and galactose units present in the carrageenan's composition. As shown in **Figure 5**, the peaks situated at 821, 1106, 1113, and 1640 cm^{-1} are attributed to the stretching of C—H, C—O or C—N bonds, —OH groups, and N—H bending, respectively.[48] The band at 844 cm^{-1} represents the C_4—O—S stretching vibration.[52] The FTIR spectra also indicated a reduction in intensity and a shift of the carrageenan —OSO_3— absorption band from 1446 to 1387 cm^{-1} following its interaction with Zn^{+2}.[53] The peaks ≈1106, 1370, 1381, and 1383 cm^{-1} are related to C=O absorption bands due to atmospheric carbon dioxide (CO_2) in the air. Broader peaks were detected between 3400 and 3600 cm^{-1} for all samples, which correspond to the asymmetric and symmetric stretching of H—O—H vibrations with visible shifts across the

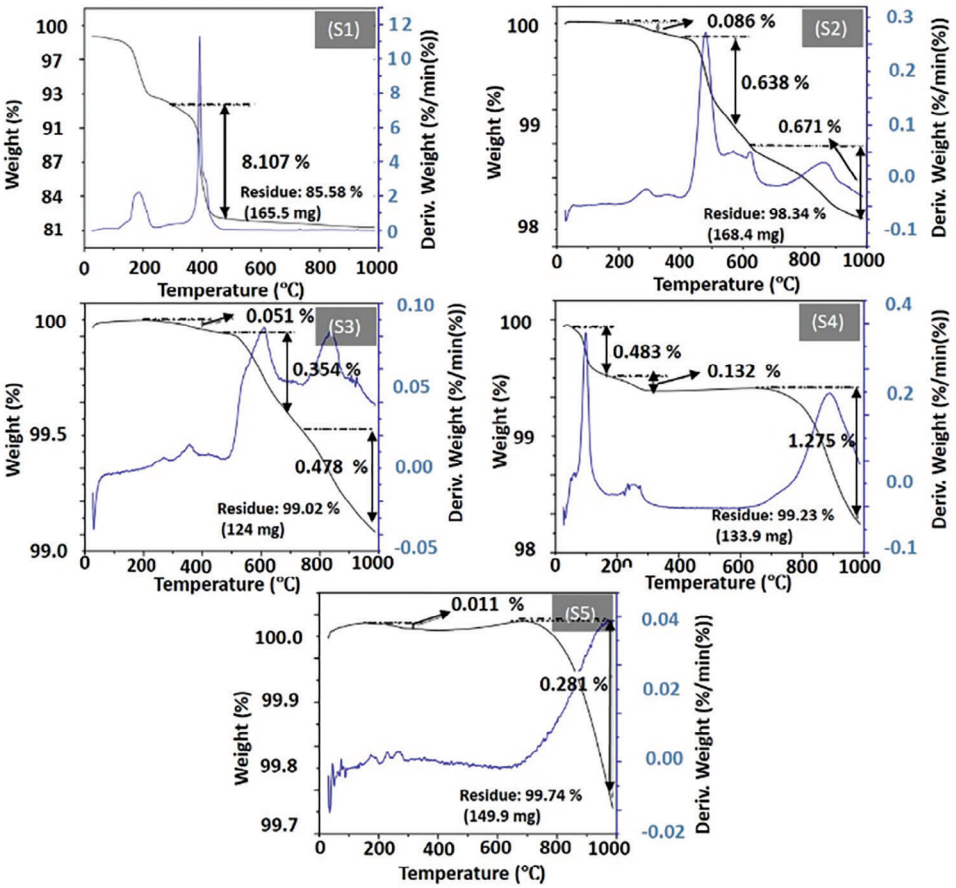

Figure 4. TGA and DTA curves of ZnO-NPs calcined at 300, 400, 500, 600, and 700 °C for the S1–S5 samples, respectively.

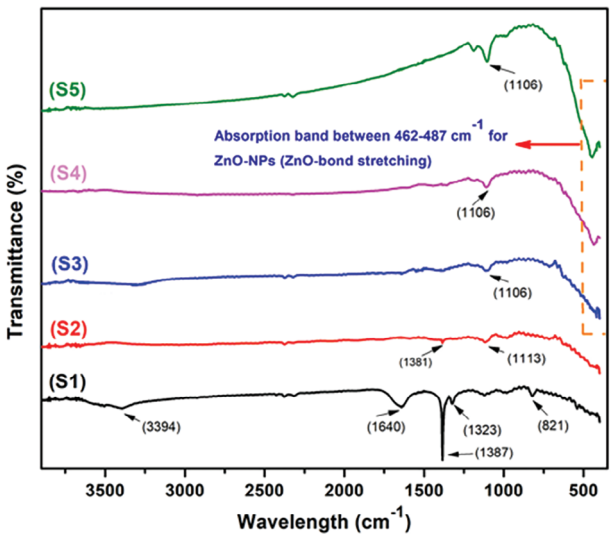

Figure 5. FTIR results of ZnO-NPs calcined at 300, 400, 500, 600, and 700 °C for the S1–S5 samples, respectively.

samples.[22] The peaks detected at 821, 1323, 1387, and 1640 cm^{-1} originate from the asymmetrical and symmetrical stretching of the zinc carboxylate.[54] Characteristic ZnO absorption bands are evident in the peaks between 407 and 487 cm^{-1} for S3, S4, and S5, indicating the successful production of ZnO-NPs.

2.5. Transmission Electron Microscopy (TEM) Analysis

Figure 6 presents TEM images for S3, S4, and S5 following calcination at 500, 600, and 700 °C, respectively. S3 and S4 showed spherical shapes, whereas, S5 displayed larger and irregular shapes. The mean diameters of S3, S4, and S5 were measured at 49 ± 12, 54 ± 13, and 62 ± 21 nm, respectively. The particle size observed in the TEM images aligns with the crystallite sizes obtained from XRD results. Notably, ZnO-NPs calcined at 600 °C (S4) showed the least aggregations and more favorable morphology than other samples. Consequently, it was chosen for further analysis.

2.6. Field Emission-Scanning Electron Microscopy (SEM) and Energy Dispersive X-Ray Spectroscopy (EDX) Analyses

Figure 7a,b showed the SEM images of the ZnO-NPs (S4) calcined at 600 °C. The images revealed consistent spherical shapes with narrow size distributions for the NPs, as clearly observed in the SEM photographs of sample S4. The particles exhibited

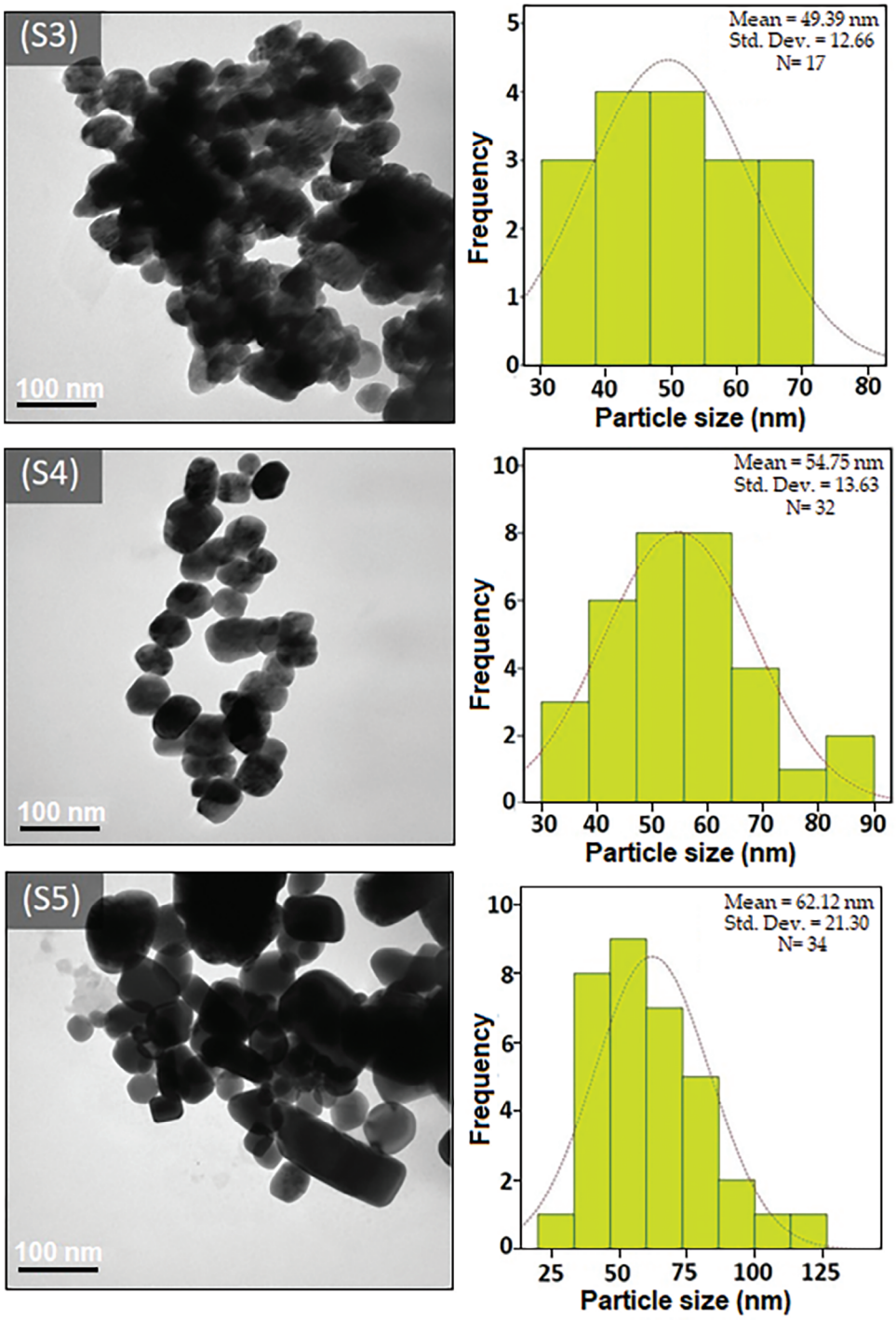

Figure 6. TEM images of ZnO-NPs calcined at 500, 600, and 700 °C for the S3–S5 samples, respectively.

an approximate size of 55 nm, which closely corresponds to the particle size observed in the TRM images of the S4 sample.

Furthermore, in Figure 7c, the EDX spectrum indicated the presence of characteristic O (25.64 wt.%) and Zn (74.36 wt.%) elements within the sample, providing further confirmation of the successful fabrication of ZnO-NPs. Comparable results were reported in a study involving ZnO-NPs stabilized by Ixora Coccinea leaf extract.[55] **Figure** 8a–c displayed the SEM images of Cs/ZnO-NPs nanomicelles fabricated from S4, demonstrating successful integration within the polymeric matrix. Additionally, elemental mapping images and EDX analysis diagram revealed the composition percentages of C, N, O, and Zn to be 15.67, 18.65, 23.45, and 42.23 wt.%, respectively. These outcomes confirmed the presence and distribution of the respective elements within

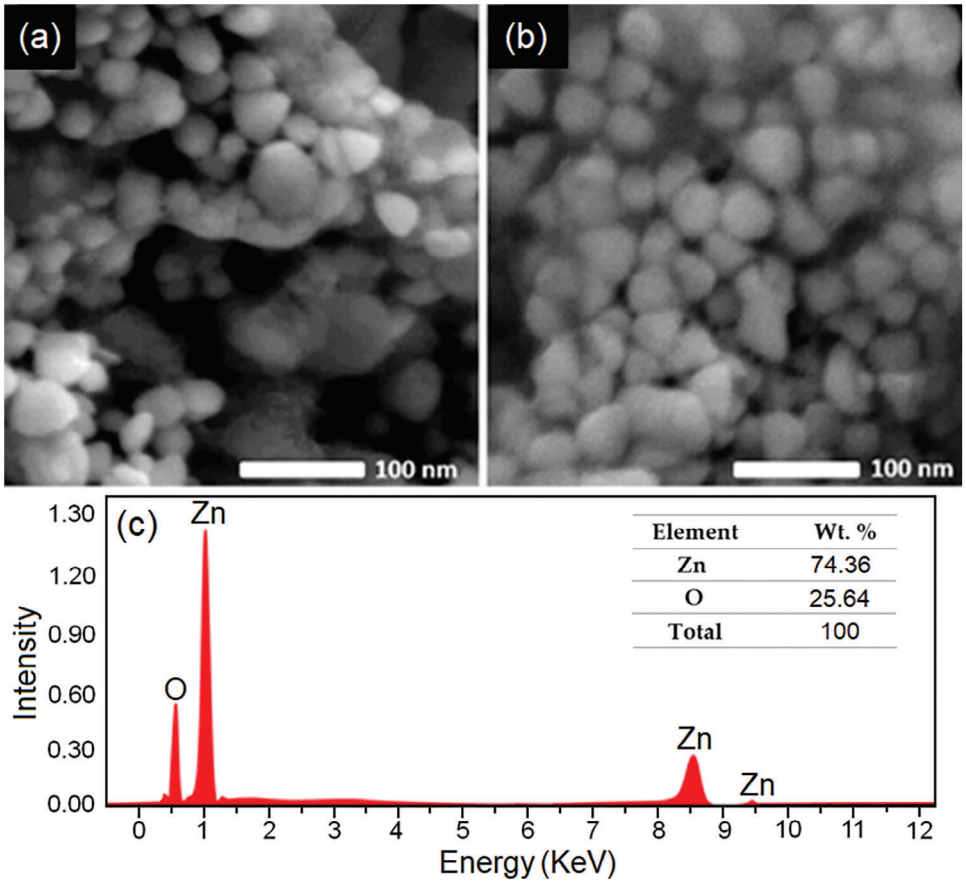

Figure 7. a,b) SEM images and c) EDX images of ZnO-NPs calcined at 600 °C (S4).

the nanomicelles. The significant proportion of Zn elements signifies the successful incorporation of ZnO-NPs into the nanomicelles, a facet of particular interest for medical applications due to their unique properties. Furthermore, the characterization of Cs/ZnO-NPs nanomicelles using SEM and EDX analysis provided valuable insights into their structure and composition, enhancing our understanding of their potential applications.

2.7. Physiochemical Analyses of ZnO-NPs and Cs/ZnO-NPs

Based on previous characterizations, ZnO-NPs calcined at 600 °C (S4) were identified as the optimal sample to be immersion in chitosan solution to fabricate Cs/ZnO-NPs. The ZnO-NPs synthesized at 600 °C (S4), exhibited high crystallinity, proper absorption peak in UV–vis spectra, clear Zn-O band in FTIR analysis, and superior morphological properties in comparison to the other samples. **Figure** 9a presents the FTIR spectra for Cs alone, ZnO-NPs, and Cs/ZnO-NPs.

In the FTIR spectra, Cs alone exhibited peaks at 653, 901, 1076, 1598, and 1657 cm^{-1} attributed to (N-H), ring stretching, (C—OH), (N—H), and —NHCO—, respectively. The presence of pure Cs is identified by a strong peak in the 3300–3500 cm^{-1} region, indicating the stretching vibration of the amine ($—NH_2$) group. It also exhibits a peak ≈3200–3400 cm^{-1}, corresponding to the stretching vibration of the hydroxyl (—OH) group. Additionally, a peak at ≈1650–1655 cm^{-1} corresponds to the carbonyl (—C═O) stretching vibration. Furthermore, Cs displays a peak in the range of 1040–1080 cm^{-1}, indicating the presence of glycosidic linkages (C—O—C) within its structure. In the Cs/ZnO spectra, the peak at 3430 cm^{-1} was shifted to lower wavenumbers, suggesting possible intermolecular interaction between chitosan and ZnO-NPs. The Zn-O stretching band ≈400–500 cm^{-1} in non-coated ZnO-NPs was absent in the Cs/ZnO-NPs spectra. Thus, both Cs and ZnO-NPs may have undergone structural modifications during the copolymerization process. This could involve changes in the crystalline structure, molecular conformation, or polymer chain arrangement.

These structural changes can lead to shifts in the FTIR peaks associated with specific functional groups in both chitosan and ZnO-NPs. Figure 9b displays the X-ray diffraction patterns of pure chitosan, Cs/ZnO-NPs and ZnO-NPs in the 2θ range of 5°–80°. The characteristic chitosan peaks were observed at 10.07° and 20.53°.[56] In the case of Cs/ZnO-NPs, the presence of peaks at 2θ angles of 32.00°, 34.53°, 36.35°, 47.65°, 56.68°, 63.05°, 66.53°, 68.05°, and 69.27° can be attributed to specific crystal planes, namely (100), (002), (101), (102), (110), (103), (200), (112), and (201). These findings signify the crystalline nature of ZnO-NPs, with all diffraction peaks aligning with the hexagonal wurtzite structure characteristic of ZnO (JCPDS card 36–1451).[56] In Figure 9c, no distinct absorption peaks were detected from the UV–vis analysis of pure chitosan. Nonetheless, both

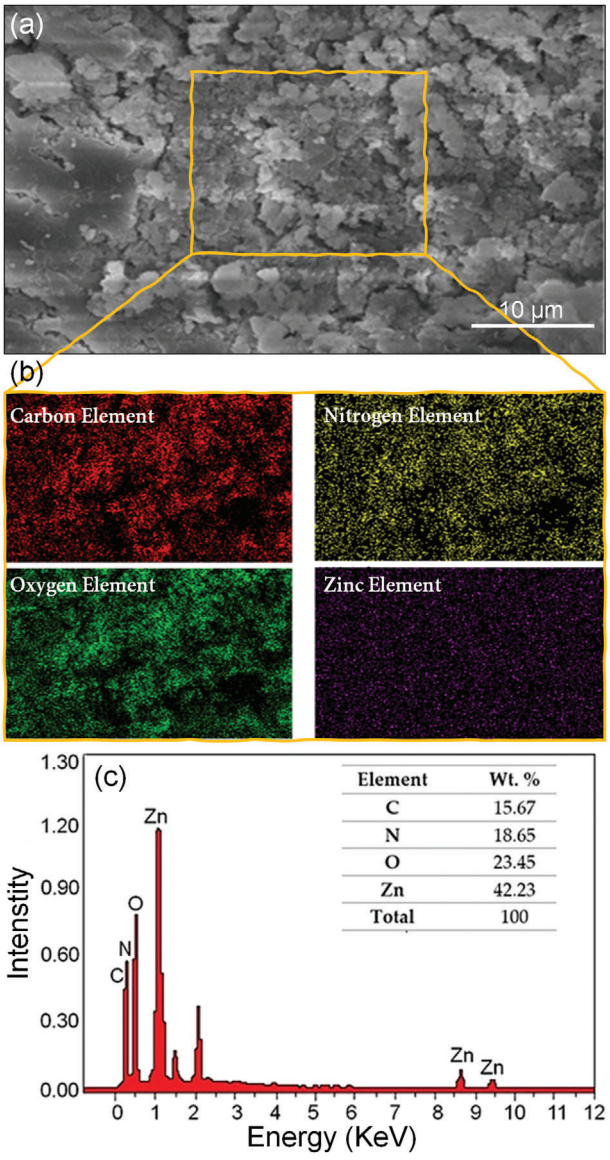

Figure 8. a) SEM image, b) elemental mapping images, including C, N, O, and Zn, together with c) EDX analysis diagram.

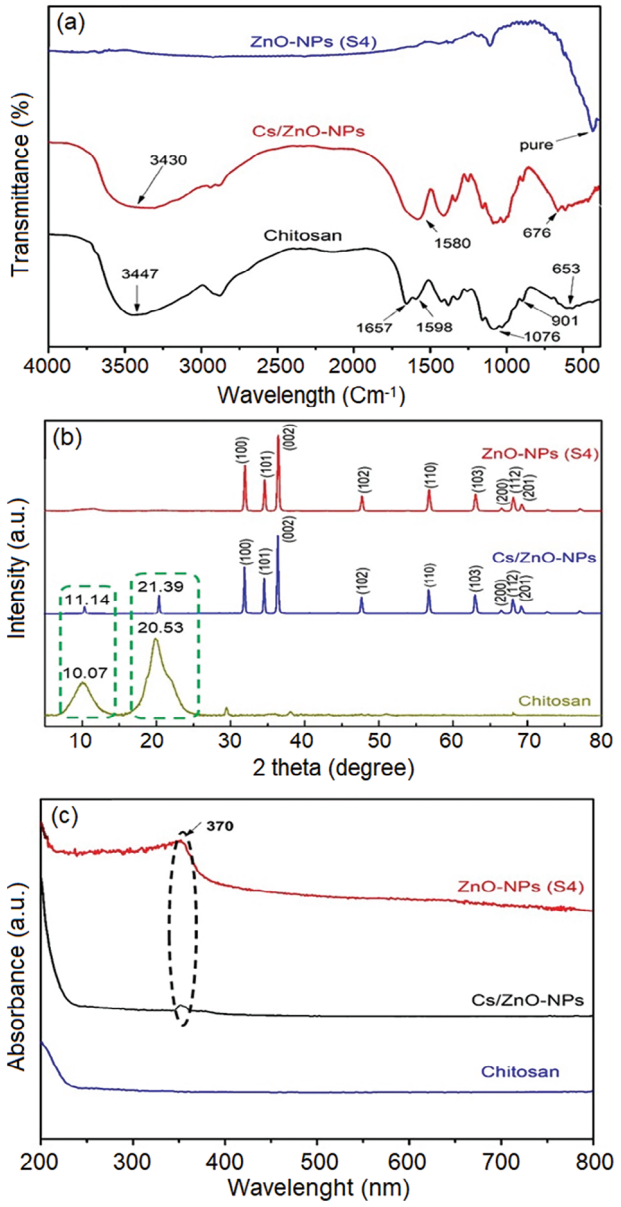

Figure 9. a) FTIR, b) XRD, and c) UV–vis spectroscopy analysis of ZnO-NPs (S4), Cs/ZnO-NPs, and chitosan.

ZnO-NPs and Cs/ZnO-NPs displayed a shared absorption peak at 370 nm. These findings collectively indicate that chitosan enveloped the ZnO-NPs.

2.8. Zeta Potential and Polydispersity Indices for ZnO and Cs/ZnO Nanoparticles

The ζ-potential, as presented in **Table 1**, offers a quantification of the surface charge, taking into consideration the potential variance between the fixed layer adhered to the surface of nanoformulations and the mobile dispersion medium. This characteristic is crucial, as it influences the cellular absorption of NPs and their stability in a colloidal environment.[57] The NPs dispersion often flocculated through and formed rapid coagulation when ζ-potential values were low, indicating aggregation tendencies, particularly for Cs/ZnO-NPs composed of large- sized ZnO-NPs. All the Cs/ZnO-NPs samples displayed ζ-potential values over +21 mV, indicating a positive charge on their surfaces, which encourages stability and prevents aggregation through electrostatic repulsion. The size of ZnO-NPs observed in the TEM analysis showed an increasing trend from S3 to S5 (49.39, 54.75, and 62.12 nm, respectively). The use of polymer medium to prepare Cs/ZnO-NPs nanomicelles enhanced the stability of the nanocolloid and prevented the precipitation of ZnO-NPs. The zeta potential results confirmed the well stability of nanomicelles across all above three samples. However, it was evident that S4 outperformed S3 and S5 in terms of colloidal stability, indicating a successful production of nanomicelles with potential applications in various therapeutic fields. These findings are promising,

Table 1. Optimal ζ-potential values for Cs/ZnO-NPs.

ZnO-NPs		ζ-potential				
		R1	R2	R3	Average	Mean ± SD
S3	1	+23.31	+24.25	+23.68	+23.50	+23.19 ± 0.31
	2	+24.74	+22.19	+22.69	+23.21	
	3	+22.57	+23.44	+22.61	+22.87	
S4	1	+27.75	+28.11	+28.63	+28.16	+27.96 ± 0.18
	2	+27.71	+28.14	+27.88	+27.91	
	3	+26.95	+28.05	+28.42	+27.81	
S5	1	+21.31	+20.75	+20.15	+20.74	+21.16 ± 0.60
	2	+20.47	+21.72	+20.53	+20.91	
	3	+21.74	+22.14	+21.67	+21.85	

SD, Standard deviation; R, Replicate.

displaying the potential of Cs/ZnO-NPs in medical research and offering opportunities for diverse therapeutic applications.

In addition to measuring size, the polydispersity indices (PDI), which range from 0.0 (completely uniform size) to 1.0 (extremely polydisperse with numerous sizes), were used to evaluate the uniformity of the particle. A high PDI value indicated that inhomogeneity in the sample made the ZnO-NP size function less useful, and thus the average size was considered to describe nanomicelle performance. This comprehensive approach provided a clearer understanding of sample homogeneity and helped to effectively evaluate its potential applications. Therefore, a lower PDI value showed a uniform size distribution and resulted in increased colloidal stability.[57] Conversely, higher PDI reflected a wider size range and decreased stability. Results herein indicated that the polydispersity index (**Table 2**), was high for the Cs/ZnO-NPs nanomicelles for S5, compared to S3 and S4. This topic revealed a substantial lack of uniformity in size distribution, clearly demonstrated by the increase in particle size observed in S5, as evident in TEM images. PDI results showed that Cs/ZnO-NPs nanomicelles for S3 had an average value of 0.61, which decreased to 0.41 for S4, indicating high colloidal stability. As a ZnO-NPs particle size increased in S5, the PDI value increased to 0.74, which indicated a decrease in nanomicelle stability. These

Table 2. Optimal polydispersity indices values for Cs/ZnO-NPs.

ZnO-NPs		PDI				
		R1	R2	R3	Average	Mean ± SD
S3	1	0.646	0.631	0.583	0.623	0.61 ± 0.02
	2	0.618	0.633	0.502	0.581	
	3	0.647	0.575	0.643	0.624	
S4	1	0.411	0.375	0.468	0.418	0.41 ± 0.01
	2	0.369	0.410	0.462	0.414	
	3	0.331	0.430	0.407	0.389	
S5	1	0.701	0.684	0.735	0.707	0.74 ± 0.06
	2	0.741	0.622	0.711	0.691	
	3	0.780	0.712	0.929	0.807	

SD, Standard deviation; R, Replicate; PDI, polydispersity indices.

Table 3. Inhibitory concentration $(IC)_{50}$ values of ZnO-NPs and Cs/ZnO-NPs in the tested cell lines in 2D monolayers and 3D spheroid models.

Cells	Model	IC_{50} [μg mL^{-1}]	
		ZnO	Cs/ ZnO
293T (normal)	2D monolayer	>125	>125
A549	2D monolayer	>125	37.18
	3D spheroid	41.17	24.71
MCF7	2D monolayer	>125	38.38
	3D spheroid	46.99	45.05
RD	2D monolayer	65.87	25.25
	3D spheroid	>125	>125

achievements highlight again the crucial relationship between PDI and nanocolloidal stability. Therefore, the optimization of achieving lower PDI values has led to the preparation of more stable nanocolloids that have been useful for cancer treatment applications.

2.9. Cytotoxicity Activities of ZnO-NPs and Cs/ZnO-NPs

ZnO-NPs showed promise in cancer treatment by selectively targeting tumor cells through enhanced uptake via leaky membranes, intracellular disruption via ROS generation, DNA damage, mitochondrial interference, and tailored properties such as size and surface chemistry. Also, binding target molecules to ZnO-NPs surfaces aimed to boost selectivity and efficacy in treatment.[58,47] In this study, both ZnO-NPs (S4) and Cs/ZnO-NPs exhibited negligible cytotoxic effects of 11.3% and 18.7%, respectively at 125 μg mL^{-1}, which is the highest test concentration, in embryonic normal human kidney cells (293T) as shown in **Figure 10**a. In contrast, the NPs showed dose-dependent killing effects on A-549, MCF7, and rhabdomyosarcoma (RD) cancer cells (Figure 10b–d).

Coating ZnO-NPs with chitosan was found to enhance killing effects on the cancer cells in both models, except in RD 3D spheroid models. At 125 μg mL^{-1}, Cs/ZnO NPs exhibited 62.8%, 73.1%, and 75% killing in A549, MCF7 and RD monolayer cells, respectively. The anticancer effect was retained in A549 spheroids (64%) and slightly reduced in MCF spheroids (66.6%). However, the anticancer effect in RD spheroid model was greatly reduced to 20.3%. Interestingly, the uncoated NPs showed a higher killing effect (35.3%). This could be due to the highly complex tissue architecture of tumor spheroid that poses a challenge for the Cs/ZnO NPs to penetrate and enter the necrotic core of spheroids to completely kill off all the cancer cells. **Table 3** summarizes the IC_{50} concentrations against all the tested cells. When comparing the IC_{50} of two NPs in 3D spheroids models, Cs/ZnO showed the lowest IC_{50} in A549 (24.71 μg mL^{-1}) followed by in MCF7 (45.05 μg mL^{-1}), but the IC_{50} in RD spheroids was more than 125 μg mL^{-1}.

Numerous studies have pointed out that a prevalent biochemical function of NPs involves elevating ROS, which in turn heightens oxidative stress within cells, potentially causing harm to cellular components like proteins, lipids, and DNA. Recently, similar results have been reported the anticancer

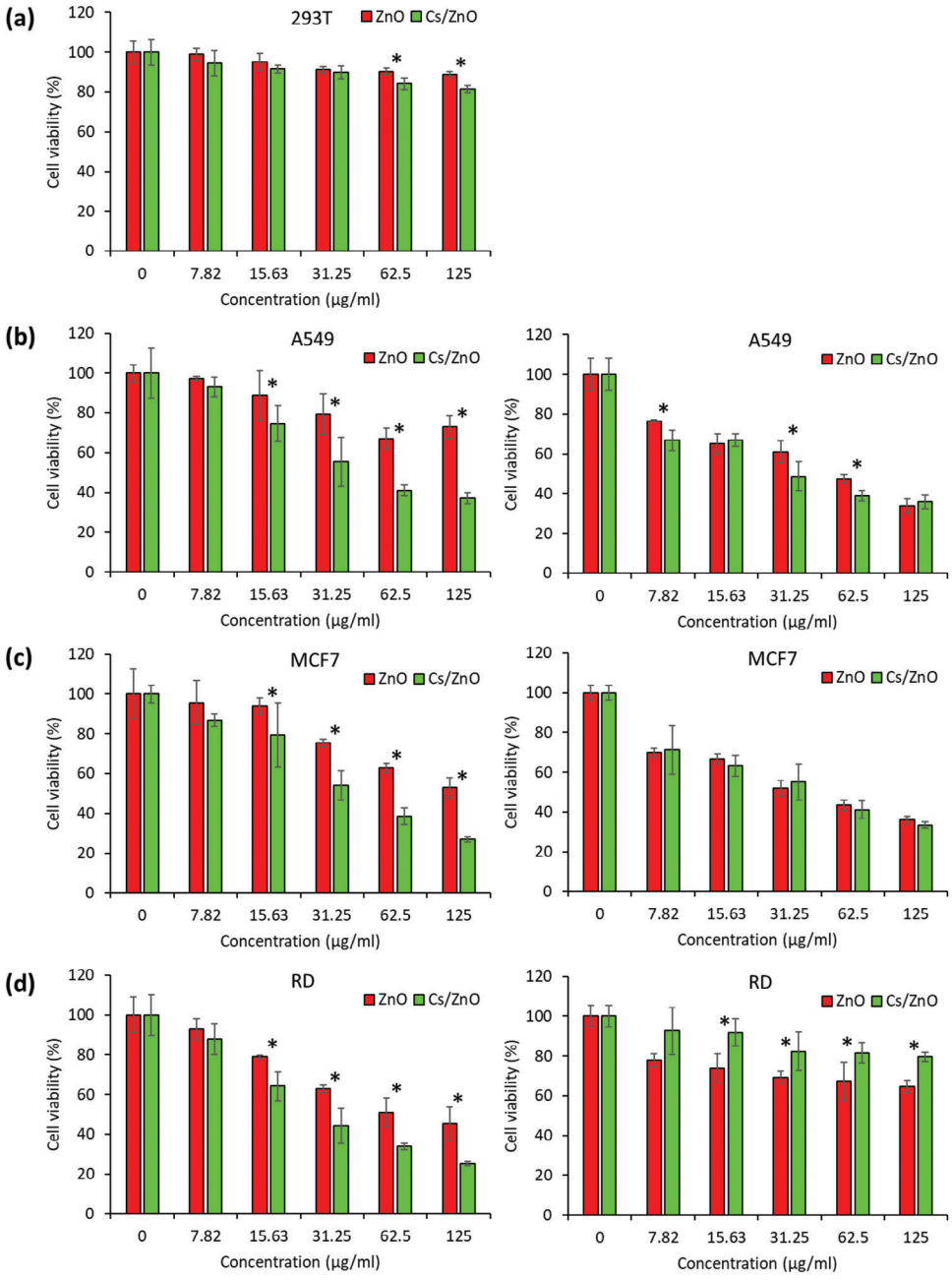

Figure 10. Cytotoxicity effects of ZnO-NPs and Cs/ZnO-NPs against a) 293T normal cell, and cancer cells b) A-549, c) MCF7 and d) RD in 2D monolayer (left panel) and 3D spheroid (right panel) models. Statistical significance was assessed using a two-way ANOVA analysis. $^{*}P \leq 0.05$.

effects of curcumin-loaded zinc oxide against RD cell lines.[59] In a separate study, zinc oxide nanorods (NRs) exhibited multifunctional properties in killing C2C12 myoblast cancer cells by upregulating caspases 3 and 7 which induce cell apoptosis.[58] The cytotoxic effect of ZnO-NPs against colorectal cancer cells, Caco-2 was also demonstrated.[60] Song and co-workers also reported that the ZnO-NPs depleted the superoxide dismutase (SOD) level and increased the ROS level in the Caco-2 intestinal cells, which suggested of accumulated oxidative stress.[61] In another study, significant cytotoxic effect was observed on MCF7 and metastatic MDA-MB-231 breast cancer cell lines treated with ZnO quantum dots (QD) with high biocompatibility toward HEK-293 normal cells.[60] The ZnO QD induced nuclear fragmentation, induced apoptosis through Bax and Bcl-2 proteins, induced cell cycle arrest at G0/G1 phase, and decreased cell proliferation and migration in both breast cancer cells.[62] Increased level of anticancer effect of Cs/ZnO-NPs compared to ZnO-NPs indicates a remarkable biocompatibility between ZnO-NPs and the cells. The therapeutic efficacy of chitosan-based NPs might stem from the interaction between the positive charge of chitosan and the negative charge on the surface of tumor cells.[32] The use of chitosan increased the surface charge, hence improving

cell absorption and antitumor action.[63] The increase molecular weight of chitosan in the Cs/ZnO-NPs could also improve the water solubility and potentially the circulation time in blood.[64] Our results strongly suggest ZnO- and Cs/ZnO-NPs as potential biocompatible NPs for anticancer applications. However, further studies are required to evaluate the target specificity, cellular uptake and bio-distribution of these NPs. The bioavailability, stability, and blood circulation experiments of the Cs/ZnO must also be studied to further explore the potential of the NPs.

3. Conclusion

In conclusion, this study explored the fabrication and characterization of ZnO-NPs, as well as their nanomicelles of Cs/ZnO-NPs for potential application in cancer treatment. The ZnO-NPs were successfully synthesized using a carrageenan medium and subjected to annealing at various temperatures. XRD and FTIR analyses confirmed the high crystallinity and purity of ZnO-NPs, particularly evident at annealing temperatures of 500, 600, and 700 °C. The most suitable temperature for further investigation was determined to be 500 °C (S3), based on XRD and FTIR data. TEM and SEM results revealed spherical and hexagonal shapes of the ZnO-NPs synthesized within 500 to 700 °C. The successful formation of Cs/ZnO-NPs was confirmed using FTIR, XRD, and EDX analysis. Notably, the nanomicelles exhibited favorable colloidal stability, particularly at 600 °C (S4), as evidenced by a low PDI value of 0.41. The ZnO-NPs demonstrated potent cytotoxicity against diverse cancer cell lines. The Cs/ZnO-NPs showed higher killing activity compared to ZnO-NPs against the cancer cells. This effect was especially pronounced at a concentration of 125 µg mL^{-1}. Overall, these findings highlight the potential of green-synthesized nanomicelles of Cs/ZnO-NPs as a promising and cost-effective nano-therapeutic agent for innovative and complementary cancer treatment in the clinical stage. The well-controlled synthesis and enhanced cytotoxicity exhibited by this type of nanomicelles pave the way for exciting avenues of research and development in the field of nanomedicine for comprehensive cancer care.

4. Experimental Section

Materials: Zinc nitrate hexahydrate ($Zn(NO_3)_2{\cdot}6H_2O$) at a purity of 98% was acquired from R&M Chemicals, located in the United Kingdom. The k-carrageenan was obtained from Sigma, grade type (CAS 9000-07-1) (95%). Low molecular weight chitosan and glacial acetic acid (HAC, purity 99%) were sourced from Sigma–Aldrich in the USA. Furthermore, all aqueous solutions were meticulously prepared using double-distilled water.

Green Synthesis of ZnO Nanoparticles: The synthesis of ZnO-NPs involved the utilization of both sol–gel and combustion methods. To commence the process, a solution was prepared by dissolving 4.5 g of $Zn(NO_3)_2{\cdot}6H_2O$ in 10 mL of distilled water. Subsequently, this solution was combined with another solution consisting of 0.2 g of κ-carrageenan dissolved in 40 mL of water. The resulting mixture underwent stirring at 60 °C for 12 h, yielding a gel-like solution. This gel was subsequently distributed across five separate Petri dishes and subjected to annealing at distinct temperatures (300, 400, 500, 600, and 700 °C) in an oven for 60 min, resulting in the production of powdered ZnO-NPs designated as S1, S2, S3, S4, and S5 respectively. These ZnO-NPs were preserved at 4 °C for subsequent experimentation.

Preparation of Chitosan-Coated ZnO Nanoparticles: Chitosan-coated ZnO-NPs, denoted as Cs/ZnO-NPs, were formulated through a process involving the dissolution of 0.2 g of ZnO-NPs (S4) in 20 mL of a 1% acetic acid (HOAc) solution containing 0.02 g of chitosan. After being subjected to 2 h of stirring at 60 °C, the NPs were subsequently precipitated by centrifugation at 6000 rpm for 10 min. Subsequently, they were rinsed with distilled water and dried at 50 °C in preparation for further analysis.

Characterization of ZnO and Cs/ZnO Nanoparticles: The structural properties of the NPs were examined using PANalytical X'Pert PRO-XRD equipment, employing Cu Kα radiation ($\lambda = 0.15406$ nm), with an applied current of 20 mA and an accelerating voltage of 45 kV. The analysis covered a 2θ range from 5° to 80°, with a scanning rate of 2θ min^{-1}. The crystalline size (D) of the NPs was determined using Scherrer's Equation (1).[65]

$$\text{Crystallite size} = \frac{0.9 \times \lambda}{\beta \times \cos\theta} \quad (1)$$

With a wavelength (λ) of 0.1540 nm, a correction factor (k) of 0.91, θ representing the diffraction angle in radians, and β indicating the full width at half maximum, the crystalline size (D) of the NPs was calculated using Scherrer's equation. To affirm the nature of the ZnO-NPs, UV–vis spectra were obtained using a UV-1800 spectrophotometer from Shimadzu Japan, covering the wavelength range of 220–800 cm^{-1}. The determination of the samples' bandgap was performed through Tauc's plot, utilizing the following Equation (2):

$$(ah\upsilon)\,2 = A\,(hv - Eg) \quad (2)$$

A is a constant, E_g represents the optical bandgap energy, h signifies Planck's constant for light energy, and α denotes the absorption coefficient. TEM (JEM-2100F-Japan) was used to determine the sample's morphology, particle size, and structure. To achieve this objective, a sample solution of ≈1.5 mg in 10 mL of distilled water was dropped onto 300-mesh copper grids. Following the drying process, TEM images were captured and subsequently analyzed.

The morphology of the samples, weighing ≈2 mg each, was assessed using a JSM-7800F Prime Schottky SEM. To this end, an accelerating voltage of 5.0 kV was employed, with a standard magnification set at 40 kV. Subsequently, SEM data was integrated with EDX analysis to characterize the chemical composition of the samples.

The functional groups present in the samples were identified using an IR Tracer-100 FTIR spectrometer (Thermo Nicolet) within the wavelength range of 400–4000 cm^{-1}. Each sample, weighing ≈5 mg, was mixed with potassium bromide (KBr) powder (500 mg) at a ratio of 1:100 w/w to create a pellet. Thermal analysis was conducted via thermogravimetric analysis (TGA) using a TGA instrument (STA F3 Jupiter) Q50 V20, employing a heating rate of 10 °C min^{-1} under a nitrogen atmosphere (10 mL min^{-1}). The ζ-potential and polydispersity index of Cs/ZnO-NPs, at a concentration of 100 µg mL^{-1}, were determined using a Zetasizer Nano ZS instrument from Malvern Instruments Ltd., based in Malvern, UK. The analysis was conducted at 25 °C, with measurements taken for 10 s each, repeated three times.

Cell Lines and Cell Culture Reagents: Rhabdomyosarcoma (RD, CCL-136), breast adenocarcinoma (MCF7, HTB-22), lung carcinoma (A-549, CCL-185), and embryonic normal human kidney (293T, CLR-3216) cell lines were acquired from the American Type Culture Collection (ATCC) and cultured following ATCC's recommended protocols. These cell lines were maintained in high-glucose Dulbecco's Modified Eagle's medium (DMEM) (#12 800, Thermo Fisher Scientific), supplemented with 10% fetal bovine serum (FBS) (#10270-106, Thermo Fisher Scientific), and 1% penicillin/streptomycin (#15140-122, Thermo Fisher Scientific).

Cytotoxicity Assay: Cytotoxicity assays were conducted to verify the cellular killing effect of the synthesized NPs using CellTiter-Glo 2.0 Luminescent Cell Viability Assay (#G9241, Promega) and according to the manufacturer's instruction.[66] In summary, 5000 cells per well (100 µL per well) were plated onto a 96-well plate and incubated for 12–16 h at 37 °C in a 5% CO_2 and 95% humidified incubator. Subsequently, the cells were exposed to samples that had been serially diluted by a factor of 2, with concentra-

tions ranging from 0 to 125 μg mL^{-1} (in 7.81 μg mL^{-1} increments), each administered at a volume of 100 μL per well. This incubation took place for a duration of 72 h at a temperature of 37 °C within a CO_2 humidified incubator. Following this, 100 μL of the detection reagent was introduced into the wells. After an incubation period of 1 h at 37 °C in a CO_2 incubator, the absorbance values were quantified using a multimode microplate reader from Tecan. Ultimately, the dose-response curve was constructed by determining the percentage of cell viability through the utilization of the equation provided below Equation (3):

$$\%\text{Cell viability} = (\text{relative luminescence unit (RLU) of sample well (mean)}) / (\text{relative luminescence unit (RLU) of control well (mean)}) \times 100 \quad (3)$$

Acknowledgements

The authors extend their sincere appreciation to the Technical University of Munich for their invaluable support in facilitating the publication of this research. Gratitude is also expressed to the Malaysia–Japan International Institute of Technology (MJIIT) for generously providing laboratory resources and instrumental analysis capabilities. The financial aspects of this study were bolstered by a research grant from Takasago Thermal Engineering Co. Ltd. (grant number: R.K.130000.7343.4B422), for which the authors are truly grateful. The role of each author in the writing of this paper is listed in order.

Conflict of Interest

The authors declare no conflict of interest.

Author Contributions

H.H., M.Y., and A.K., K.S. performed conceptualization. H.H., M.Y., B., S.Y.T., Y.S.W., A.A., and K.S. performed data curation. H.H., S.D.J., M.Y., B., Y.S.W., A.A., and K.S. performed formal analysis. K.S. performed funding acquisition. S.K. and K.S. performed the investigation. H.H., S.D.J., M.Y., B., S.Y.T., Y.S.W., A.A., A.K., and K.S. performed methodology. H.H., B., S.Y.T., and K.S. performed project administration. S.Y.T. and K.S. acquired resources. H.H., M.Y., A.A., S.K., A.K., and K.S. acquired the software. K.S. performed supervision. H.H., S.Y.T., Y.S.W., S.K., M.Y., and K.S. performed validation. H.H., S.K., A.K., and K.S. performed visualization. H.H., S.D.J., B., S.Y.T., and K.S. wrote and prepared the original draft. H.H., A.K., and K.S. wrote, reviewed, and edited the final manuscript. All authors have read and agreed to the published version of the manuscript.

Data Availability Statement

The data that support the findings of this study are available from the corresponding author upon reasonable request.

Keywords

cancer treatment, cytotoxicity, innovative therapy, nanomedicine, ZnO nanoparticles

Received: January 25, 2024
Revised: March 13, 2024
Published online: March 27, 2024

[1] K. Shameli, M. B. Ahmad, S. D. Jazayeri, S. Sedaghat, P. Shabanzadeh, H. Jahangirian, M. Mahdavi, Y. Abdollahi, *Int. J. Mol. Sci.* **2012**, *13*, 6639.
[2] R. Wahab, J. Ahmad, N. Ahmad, *Colloids Surf A Physicochem Eng Asp* **2019**, *583*, 123953.
[3] H. Hamrayev, K. Shameli, M. Yusefi, *J Adv Res Micro Nano Eng* **2020**, *2*, 1.
[4] P. K. Mishra, H. Mishra, A. Ekielski, S. Talegaonkar, B. Vaidya, *Drug Discov Today* **2017**, *22*, 1825.
[5] A. Karakecili, S. Korpayev, H. Dumanoglu, S. Alizadeh, *J. Biotechnol.* **2019**, *303*, 8.
[6] A. K. Barui, R. Kotcherlakota, C. R. Patra, *Inorganic Frameworks as Smart Nanomedicines*, (Ed: A. M. Grumezescu), William Andrew Publishing, Norwich, NY **2018**.
[7] D. Mafra, N. A. Borges, B. Lindholm, P. G. Shiels, P. Evenepoel, P. Stenvinkel, *Nat Rev Nephrol* **2021**, *17*, 153.
[8] L. Wan, M. Yang, *IOP Conf Ser Mater Sci Eng* **2020**, *772*, 012050.
[9] C. L. Kuo, C. L. Wang, H. H. Ko, W. S. Hwang, K. M. Chang, W. L. Li, H. H. Huang, Y. H. Chang, M. C. Wang, *Ceram. Int.* **2010**, *36*, 693.
[10] E. D. M. Isa, K. Shameli, H. J. Ch'ng, N. W. C. R. Jusoh, Hazan, *Adv. Powder Technol.* **2021**, *32*, 2398.
[11] M. Omichi, Y. Ueki, N. Seko, Y. Maekawa, *Polymers* **2019**, *11*, 1373.
[12] A. Menazea, N. S. Awwad, *J Mater Res Technol* **2020**, *9*, 9434.
[13] M. T. Noman, M. Petrů, *Nanomater* **2020**, *10*, 1661.
[14] F. Moradnia, S. T. Fardood, A. Ramazani, S. Osali, I. Abdolmaleki, *Micro Nano Lett* **2020**, *15*, 674.
[15] E. D. M. Isa, K. Shameli, N. W. C. Jusoh, R. Hazan, *J Nanostructure Chem* **2021b**, *11*, 187.
[16] J. Wojnarowicz, T. Chudoba, W. Lojkowski, *Nanomaterials* **2020**, *10*, 1086.
[17] H. Hamrayev, K. Shameli, S. Korpayev, *J Res Nanosci Nanotechnol* **2021**, *1*, 62.
[18] Z. Ajdari, H. Rahman, K. Shameli, R. Abdullah, M. Abd Ghani, S. Yeap, S. Abbasiliasi, D. Ajdari, A. Ariff, *Molecules* **2016**, *21*, 123.
[19] A. M. Awwad, M. W. Amer, N. M. Salem, A. O. Abdeen, *Chem Int* **2020**, *6*, 151.
[20] K. Rambabu, G. Bharath, F. Banat, P. L. Show, *J. Hazard. Mater.* **2021**, *402*, 123560.
[21] P. Amuthavalli, J. S. Hwang, H. U. Dahms, L. Wang, J. Anitha, M. Vasanthakumaran, A. D. Gandhi, K. Murugan, J. Subramaniam, M. Paulpandi, *Sci. Rep.* **2021**, *11*, 8837.
[22] S. N. A. M. Sukri, K. Shameli, M. M. T. Wong, S. Y. Teow, J. Chew, N. A. Ismail, *J. Mol. Struct.* **2019**, *1189*, 57.
[23] S. Umavathi, M. Ramya, C. Padmapriya, K. Gopinath, *J Biol Act Prod Nat* **2020**, *10*, 153.
[24] H. Hamrayev, K. Shameli, *IOP Conf Ser Mater Sci Eng* **2021**, *1051*, 012088.
[25] S. H. Mohd-Taib, K. Shameli, P. Moozarm-Nia, M. Etesami, M. Miyake, R. Rasit-Ali, E. Abouzari-Lotf, Z. Izadiyan, *J. Taiwan Inst. Chem. Eng.* **2019**, *95*, 616.
[26] M. Yusefi, K. Shameli, Z. Hedayatnasab, S. Y. Teow, U. N. Ismail, C. A. Azlan, A. Rasit-Ali, *Res. Chem. Intermed.* **2021**, *47*, 1789.
[27] M. J. Khan, S. Kumari, K. Shameli, J. Selamat, A. Qurni, *Materials* **2019**, *12*, 2382.
[28] A. M. Abdelgawad, M. E. El-Naggar, D. A. Elsherbiny, S. Ali, M. S. Abdel-Aziz, Y. K. Abdel-Monem, *J. Environ. Chem. Eng.* **2020**, *8*, 104276.
[29] H. Hamrayev, K. Shameli, M. Yusefi, S. Korpayev, *J. Res. Nanosci. Nanotechnol.* **2021**, *3*, 1.
[30] E. Nourmohammadi, R. Kazemi-Oskuee, L. Hasanzadeh, M. Mohajeri, A. Hashemzadeh, M. Rezayi, M. Darroudi, *Ceram. Int.* **2018**, *4*, 19570.
[31] M. Yusefi, M. S. Lee-Kiun, K. Shameli, S. Y. Teow, R. R. Ali, K. K. Siew, H. Y. Chan, M. M. T. Wong, W. L. Lim, K. Kuča, *Carbohydr. Polym.* **2021**, *273*, 118523.
[32] M. Yusefi, H. Y. Chan, S. Y. Teow, P. Kia, M. Lee-Kiun Soon, N. A. B. C. Sidik, K. Shameli, *Nanomater* **2021**, *11*, 1691.

[33] S. Liu, J. Zhang, X. Cui, Y. Guo, X. Zhang, W. Hongyan, *Colloids Surf A Physicochem Eng Asp* **2016**, *490*, 91.
[34] M. Akbarian, S. Mahjoub, S. M. Elahi, E. Zabihi, H. Tashakkorian, *Colloids Surf B* **2020**, *186*, 110686.
[35] S. Korpayev, A. Karakeçili, H. Dumanoğlu, S. I. A. Osman, *Biotechnol. J.* **2021**, *16*, 2100046.
[36] M. Yusefi, K. Shameli, O. S. Yee, S. Y. Teow, Z. Hedayatnasab, H. Jahangirian, T. J. Webster, K. Kuča, *Int. J. Nanomed.* **2021**, *16*, 2515.
[37] M. Magro, F. Vianello, *Nanomater* **2019**, *9*, 1608.
[38] R. Mustika, A. Wardana, *Food Res* **2020**, *4*, 1867.
[39] L. Upadhyaya, J. Singh, V. Agarwal, A. C. Pandey, S. P. Verma, P. Das, R. P. Tewari, *Process Biochem* **2015**, *50*, 678.
[40] Y. A. Selim, M. A. Azb, I. Ragab, M. H. Abd El-Azim, *Sci. Rep.* **2020**, *10*, 3445.
[41] M. Ahmar Rauf, M. Oves, F. Ur Rehman, A. Rauf Khan, N. Husain, *Biomed. Pharmacother.* **2019**, *116*, 108983.
[42] Q. Tang, H. Xia, W. Liang, X. Huo, X. Wie, *J Photochem Photobiol B* **2020**, *202*, 111698.
[43] K. Dulta, G. Koşarsoy Ağçeli, P. Chauhan, R. Jasrotia, P. K. Chauhan, *J. Inorg. Organomet. Polym. Mater.* **2021**, *31*, 180.
[44] S. Majeed, M. Danish, M. H. B. Ismail, M. T. Ansari, M. N. M. Ibrahim, *Sustain Chem Pharm* **2019**, *14*, 100179.
[45] M. Rajan, A. J. Anthuvan, K. Muniyandi, N. K. Kalagatur, S. Shanmugam, S. Sathyanarayanan, V. Chinnuswamy, P. Thangaraj, N. Narain, *Arab J Sci Eng* **2019**, *45*, 15.
[46] M. Vaghari-Tabari, D. Jafari-Gharabaghlou, M. Mohammadi, M. S. Hashemzadeh, *Biol. Trace Elem. Res.* **2023**, *202*, 1878.
[47] Y. Hu, H. R. Zhang, L. Dong, M. R. Xu, L. Zhang, W. P. Ding, J. Q. Zhang, J. Lin, Y. J. Zhang, B. S. Qiu, P. F. Wei, L. P. Wen, *Nanoscale* **2019**, *20*, 1111789.
[48] A. K. Zak, W. A. Majid, M. Mahmoudian, M. Darroudi, R. Yousefi, *Adv. Powder Technol.* **2013**, *24*, 618.
[49] S. Taghavi Fardood, A. Ramazani, S. Moradi, P. Azimzadeh-Asiabi, *J Mater Sci Mater Electron* **2017**, *28*, 13596.
[50] M. Goswami, N. C. Adhikary, S. Bhattacharjee, *Optik* **2018**, *158*, 1006.
[51] P. V. Raleaooa, A. Roodt, G. G. Mhlongo, D. E. Motaung, R. E. Kroon, O. M. Ntwaeaborwa, *Phys B: Condens* **2017**, *507*, 13.
[52] S. Abdullah, N. H. Azeman, N. N. Mobarak, M. S. D. Zan, A. A. Bakar, *Optik* **2018**, *168*, 784.
[53] M. M. Elnashar, M. A. Yassin, *Appl. Biochem. Biotechnol.* **2009**, *159*, 426.
[54] A. K. Zak, W. H. A. Majid, M. Darroudi, R. Yousefi, *Mater. Lett.* **2011**, *65*, 70.
[55] S. Rajeshkumar, S. V. Kumar, A. Ramaiah, H. Agarwal, T. Lakshmi, S. M. Roopan, *Enzyme Microb* **2018**, *117*, 91.
[56] M. M. Abdelhady, *Int J Carbohydr Chem* **2012**, *2012*, 840591.
[57] J. N. Losso, A. Khachatryan, M. Ogawa, J. S. Godber, F. Shih, *Food Chem.* **2005**, *92*, 737.
[58] J. W. Rasmussen, E. Martinez, P. Louka, D. G. Wingett, *Expert Opin Drug Deliv* **2010**, *7*, 1063.
[59] W. Perera, R. K. Dissanayake, U. Ranatunga, N. Hettiarachchi, K. Perera, J. M. Unagolla, R. De Silva, L. Pahalagedara, *RSC Adv.* **2020**, *10*, 30785.
[60] R. Wahab, Q. Saquib, M. Faisal, *Process Biochem* **2020**, *98*, 83.
[61] Y. Song, R. Guan, F. Lyu, T. Kang, Y. Wu, X. Chen, *Mutat* **2014**, *769*, 113.
[62] A. Roshini, S. Jagadeesan, Y. J. Cho, J. H. Lim, K. H. Choi, *Mater Sci Eng C* **2017**, *81*, 551.
[63] E. Bilensoy, *Expert Opin Drug Deliv* **2010**, *7*, 795.
[64] Y. Herdiana, N. Wathoni, S. Shamsuddin, I. M. Joni, M. Muchtaridi, *Polymers* **2021**, *13*, 1717.
[65] Z. Izadiyan, K. Shameli, S. Y. Teow, M. Yusefi, P. Kia, E. Rasouli, M. A. Tareq, *J. Mol. Struct.* **2021**, 131075.
[66] M. Yusefi, K. Shameli, R. R. Ali, S. W. Pang, S. Y. Teow, *J. Mol. Struct.* **2020**, *1204*, 127539.

